Available online at www.sciencedirect.com
SCIENCE DIRECT®
Journal of Solid State Chemistry 177 (2004) 45–54
JOURNAL OF SOLID STATE CHEMISTRY
http://elsevier.com/locate/jssc

$La_xSr_{2-x}Fe_yRu_{1-y}O_{4\pm\delta}$: a new family of K_2NiF_4 type oxides

A.J. Jennings,[a] S.J. Skinner,[a,*] and Örn Helgason[b]

[a] *Department of Materials, Imperial College London, Prince Consort Road, London SW7 2BP, UK*
[b] *Science Institute, University of Iceland, Dunhagi 3, Reykjavik, IS-107, Iceland*

Received 3 February 2003; received in revised form 8 May 2003; accepted 23 May 2003

Abstract

The phases $La_xSr_{2-x}Fe_yRu_{1-y}O_{4\pm\delta}$ ($x=0.2$–0.8; $y=0.6$–0.9) have been synthesized by solid-state techniques and yield tetragonal structures with *I*4/*mmm* symmetry. The oxygen stoichiometry and high-temperature structures have been examined using diffraction techniques and in situ Mössbauer spectroscopy at temperatures up to ~600°C. Furthermore, new reduced phases that adopt structures with *Immm* symmetry have been discovered. Unusual coordination numbers have been determined for the most highly reduced samples with square planar coordination evident for the *B* site cations. The reduced orthorhombic *Immm* phases were found to readily reoxidize in air to the tetragonal *I*4/*mmm* structure at relatively low temperatures of only ~500°C.

Keywords: $La_xSr_{2-x}Fe_yRu_{1-y}O_{4\pm\delta}$; *I*4/*mmm*; *Immm*; Structure and diffraction

Introduction

This work on ruthenium doped $La_xSr_{2-x}FeO_{4\pm\delta}$ stems from our interest in new oxide ion conducting systems for use in solid oxide fuel cells and ceramic oxygen generators. In particular, our initial aim was to produce new interstitial oxide containing solids that were stable over a range of oxygen partial pressures appropriate to the preparation and operation of solid oxide fuel cell (SOFC) cathodes. The main focus of this work would therefore be on the thermal stability and structural characterization of the materials.

It was envisaged that the structure of these new phases would be of the K_2NiF_4 type in common with many other lanthanide-based transition metal oxides of this stoichiometry. Indeed, it was further anticipated that the Ru doping may introduce oxygen interstitials which are of interest as interstitial containing K_2NiF_4 type oxides have received considerable attention recently as possible cathode materials in SOFCs due to the nature of the fast oxide ion conduction reported [1–4]. However, relatively few materials have been identified as having the appropriate combination of ionic and electronic conductivity to be considered for this application. It is only the $Ln_2NiO_{4+\delta}$ (*Ln* = La, Nd, Pr) materials that have shown any promise in this respect to date [5,6] and therefore it is of interest to develop new materials with optimized conduction properties. This work builds on earlier studies of the $La_xSr_{2-x}FeO_{4\pm\delta}$ series [7] and doping with ruthenium opens up interesting possibilities in terms of the oxidation states of the transition metals and our aim in this work was to make new phases and then investigate their structural properties and thermal stability prior to investigation of their electrical/ionic conduction properties.

Some previous studies on K_2NiF_4 related oxides have reported the synthesis of Sr_4FeRuO_8 (*I*4/*mmm* $a=3.9025$ Å, $c=12.5943$ Å) [8, 9], $La_{2-x}Sr_xCu_{1-y}Ru_yO_{4-\delta}$ [10] and $Sr_2Ru_{0.5}M_{0.5}O_4$ (M = Ni, Co, Ga) [11]. Battle et al. [8] made both Sr_4FeRuO_8 and Sr_3FeRuO_7 (*I*4/*mmm* $a=3.9187$ Å, $c=20.4146$ Å) by solid-state chemical techniques at 1200–1400°C. It is reported that both materials adopted the K_2NiF_4 type structure with iron and ruthenium adopting the 3+ and 5+ oxidation states, respectively. A related material, Sr_2FeRuO_6, adopts the perovskite structure, crystallizing in the I_2/c space group with cell constants of $a=5.5092$ Å, $b=5.5138$ Å, $c=7.8752$ Å and $\beta=90.11°$ [12]. Perhaps of more direct relevance to the present work is that of Ebbinghaus et al. [10] who investigated 90 members of the system $La_{2-x}Sr_xCu_{1-y}Ru_yO_{4-\delta}$ producing many

*Corresponding author. Fax: +44(0)20-7584-3194.
E-mail address: s.skinner@imperial.ac.uk (S.J. Skinner).

0022-4596/$ - see front matter © 2003 Elsevier Inc. All rights reserved.
doi:10.1016/S0022-4596(03)00305-0

single-phase materials from solid-state techniques. Unfortunately, they provided very little structural detail with no mention of the space groups used in the refinements of X-ray powder diffraction data.

In this work we have successfully synthesized the compounds $La_xSr_{2-x}Fe_yRu_{1-y}O_{4\pm\delta}$ ($x=0.2$–0.8; $y=0.6$–0.9) and in the process of investigating the stability and structure of these phases have discovered a family of new structurally related materials produced by reduction of the parent oxides.

2. Experimental

Synthesis of a number of compositions has been investigated and single-phase products obtained for the compositions $La_{0.8}Sr_{1.2}Fe_{0.9}Ru_{0.1}O_{4\pm\delta}$, $La_{0.6}Sr_{1.4}Fe_{0.8}Ru_{0.2}O_{4\pm\delta}$, $La_{0.4}Sr_{1.6}Fe_{0.7}Ru_{0.3}O_{4\pm\delta}$ and $La_{0.2}Sr_{1.8}Fe_{0.6}Ru_{0.4}O_{4\pm\delta}$. Stoichiometric quantities of La_2O_3 (previously dried at 700°C for 12 h), Fe_2O_3, RuO_2 (previously dried at 500°C for 12 h) and $SrCO_3$ were ground in ethanol to achieve a homogenous mixture. The resultant powder was heated at 300°/h to 750°C in a muffle furnace and allowed to react for 12 h. The powder was reground and heated for a further 12 h at 1050°C. After a further regrinding the powder was pelletized and heated to 1200°C for 12 h, to 1250°C for 12 h and finally annealed at 1350°C for 24 h. The mixing of the reactants is very slow and a prolonged synthesis is essential to produce a single-phase product. Frequent intermittent regrindings are also an essential requirement for synthesis of these materials. The progress of the reactions was monitored using powder X-ray diffraction using a Phillips PW1700 series automated powder diffractometer with Cu$K\alpha$ radiation and a graphite secondary crystal monochromator.

Once single-phase products had been obtained the stability and structure of these phases was investigated. Detailed structural investigations were performed using X-ray diffraction on Station 2.3 at Daresbury Laboratory synchrotron radiation source with a wavelength of 1.401359 Å calibrated with a silicon standard. In situ high-temperature powder X-ray diffraction was carried out at Imperial College using a Phillips X'Pert MPD diffractometer with a Bühler HDK 2.4 high-temperature chamber and Cu$K\alpha$ radiation and a graphite secondary crystal monochromator. Thermogravimetric analysis was carried out using a Stanton Redcroft 780 series simultaneous thermal analyser (TGA/DTA) operating under H_2/N_2 gas flow or in air. To establish the oxidation states of the transition metals iodometric titrations [13] were used and complemented with ^{57}Fe Mössbauer spectroscopy studies performed at the University of Iceland in order to probe the iron environment and oxidation state.

3. Results and discussion

(i) *Samples prepared and characterized in air*: Attempts were made to synthesize samples with a number of different stoichiometries as the variable oxidation states exhibited by the transition metals, iron and ruthenium, suggested that a range of stoichiometries could be produced including either cation or anion vacancies. Furthermore, as the cation ratios were altered the possibility existed of structural modifications occurring that could influence the electronic/ionic mobility of the phase of interest. However, the only samples successfully synthesized as a single phase were $La_{0.8}Sr_{1.2}Fe_{0.9}Ru_{0.1}O_{4\pm\delta}$, $La_{0.6}Sr_{1.4}Fe_{0.8}Ru_{0.2}O_{4\pm\delta}$, $La_{0.4}Sr_{1.6}Fe_{0.7}Ru_{0.3}O_{4\pm\delta}$ and $La_{0.2}Sr_{1.8}Fe_{0.6}Ru_{0.4}O_{4\pm\delta}$. The final member of this series would be '$Sr_2Fe_{0.5}Ru_{0.5}O_4$' and the compound Sr_4FeRuO_8 has already been reported in the literature by Battle et al. [8] and Greatrex et al. [9]. The first member of this series is $LaSrFeO_4$ and this has also been widely reported in the literature [13,14]. Both end member materials adopt the tetragonal K_2NiF_4 type structure.

The structures of the new phases reported here were identified from initial X-ray diffraction data as adopting the K_2NiF_4 type structure and could be indexed with a tetragonal cell consistent with the *I*4/*mmm* spacegroup. Further high-resolution data were recorded, between $2\theta=10$ and 100° at a resolution of 0.01 for 1 s per step, on all four samples on Station 2.3 at the Daresbury Laboratory synchrotron radiation source in order to carry out more detailed structural characterization.

The XRD data were analyzed using a full Rietveld refinement employing the GSAS suite of programs [15]. An initial model that was consistent with previous studies of tetragonal K_2NiF_4 type oxides [16,17] was used in the refinement with lanthanum and strontium disordered on (00*z*) initially with $z\approx0.35$, iron and ruthenium disordered on (000) and the oxygen atoms sited on $(0\,\frac{1}{2}\,0)$ and (00*z*) initially with $z\approx0.16$. A good fit to the data was obtained using a shifted Cherbyshev background function and a pseudo-Voigt peak shape. However, closer inspection of the fit at this stage, particularly at high Ru contents, revealed that the peak shape of some of the reflections, did not fit well. This poor fitting resulted from a broadening of the reflections to lower values of 2θ. The reflections affected were primarily (00*l*) reflections or reflections with a high *l* component, for example, the (004) and (1,0,11) were particularly affected. Using the anisotropic peak shape matrix in the refinement improved the fit with the *L*33 component refining to a small positive value, $L33 = 0.005$ for the 40% Ru doped sample. Final refined data for $La_{0.8}Sr_{1.2}Fe_{0.9}Ru_{0.1}O_{4\pm\delta}$ and $La_{0.2}Sr_{1.8}Fe_{0.6}Ru_{0.4}O_{4\pm\delta}$ are shown in Table 1 and Fig. 1. From this analysis it is apparent that these samples are subject to some stacking faults apparently in the *c*-axis direction

Table 1
Refined data for the 10% (R_{wp} = 9.82%, R_p = 7.46%) and 40% (R_{wp} = 9.53%, R_p = 7.47%) Ru-doped samples in air

	10%Ru					40%Ru				
	x	y	z	$U_{iso} \times 100$ (Å^2)	F_{rac}	x	y	z	$U_{iso} \times 100$ (Å^2)	F_{rac}
La	0	0	0.35791 (6)	0.582 (30)	0.361 (11)	0	0	0.35423 (6)	1.189 (32)	0.045 (12)
Sr	0	0	0.35791 (6)	0.582 (30)	0.639 (11)	0	0	0.35423 (6)	1.189 (32)	0.955 (12)
Fe	0	0	0	0.43 (8)	0.947 (8)	0	0	0	0.55 (6)	0.621 (10)
Ru	0	0	0	0.43 (8)	0.53 (8)	0	0	0	0.55 (6)	0.379 (10)
O1	0	0.5	0	1	1	0	0.5	0	1	0.881 (10)
O2	0	0	0.1646 (5)	1	1	0	0	0.1609 (4)	1	0.992 (9)

and could be due to incomplete mixing of the iron and ruthenium in the lattice such that they are not fully disordered on the (000) site. It could also result from the presence of small amounts of a solid solution series of phases some of which are richer in ruthenium accompanied by a majority phase.

The refined cell constants for all compositions are given in Table 2 and the variation of the cell constants with Ru content shown in Fig. 2. Both a and c, and therefore the c/a ratio, were found to vary linearly with the Ru content of the samples. The cell constant variations are therefore clearly dependent on the oxidation state of the transition metal ions, with significant variation on increasing Ru content. The ionic radius of the transition metal and the strength and length of the bonds it forms with oxygen are known to be dependent on the oxidation state or states exhibited. In particular, a would be expected to be affected by the transition metal as the perovskite slabs in the K_2NiF_4 type structure link through corner sharing in the ab plane. The c-axis, on the other hand, should be strongly dominated by the (La/Sr)–O bonds. Indeed through consideration of the unit cell parameters (Fig. 2) and the (Fe/Ru)–O bond lengths (Fig. 3) it is apparent that the a cell parameter and the (Fe/Ru)–O1 bond length are closely related.

As the Ru content increases in these samples the strontium content of the material also increases and hence the replacement of La with Sr would be expected to result in an expansion of the c-axis. From Fig. 2 this is clearly not the case. However, careful examination of the individual bond lengths (Table 3) indicates that on increasing Sr content the (La/Sr)–O1 and (La/Sr)–O2 bonds do indeed increase as expected, but that the decrease in the length of the (Fe/Ru)–O2 bonds is of far greater magnitude and evidently controls the c-axis contraction. Furthermore, as in the undoped materials [7], the (Fe,Ru)O_6 octahedra are distorted, but the distortion is of a lower magnitude than was observed in the 100% Fe materials and indeed decreases with increasing Ru content (Fig. 3 and Table 3).

The thermal stability of the new ruthenium containing phases was investigated using high-temperature X-ray diffraction where data were collected on samples in situ while heating up to temperatures of 1000°C. Also TGA and DTA analysis in air has been used to ensure there are no subtle phase transitions occurring that could not be detected in the XRD measurements and to monitor any likely oxygen stoichiometry changes. In both air and vacuum the samples are stable at temperatures of up to 1000°C with no sign of any phase transitions occurring.

The unit cell parameters were determined as a function of temperature using Lebail extractions [18] on the data collected and show a linear increase with temperature for both the a and c parameters, as shown in Fig. 4 for $La_{0.7}Sr_{1.3}Fe_{0.8}Ru_{0.2}O_4$. The TGA data recorded in air showed no mass change on heating. Hence, it is concluded that these Ru doped phases are structurally stable and do not appear to show any sign of oxygen uptake leading to oxygen hyperstoichiometry.

In an attempt to determine the oxidation state of the transition metals in these materials several different characterization techniques have been used. Iodometric titrations were performed, ^{57}Fe Mössbauer spectroscopy studies were used to investigate the iron environment and oxidation state and thermogravimetric analysis in reducing conditions was also used to determine the oxidation states of the metals. However with both iron and ruthenium showing variable oxidation states in their compounds it has been challenging to determine which oxidation states were adopted. From the iodometric titrations it appears that the ruthenium is in the +5 oxidation state as would be expected. This has been previously attributed as the oxidation state Ru adopts in Sr_4FeRuO_8 and other Ru containing oxide materials [8], although Greatrex et al. suggest a mixed $Ru^{IV/V}$ state in $Sr_2Fe_xRu_{1-x}O_4$ [9]. However iron appears to adopt +2, +3 and +4 oxidation states in these samples. This is supported by evidence from both the iodometric titrations, Mössbauer spectroscopy data. In Table 4 the data obtained from the titrations, Mössbauer spectra and TGA is compared. From this the TGA data suggests that under reducing conditions, up to 700°C, the weight loss observed can be attributed to reduction of ruthenium from the +5 oxidation state to the +3 oxidation state.

The Mössbauer spectroscopy data that have been recorded for the 10% and 30% Ru doped phases,

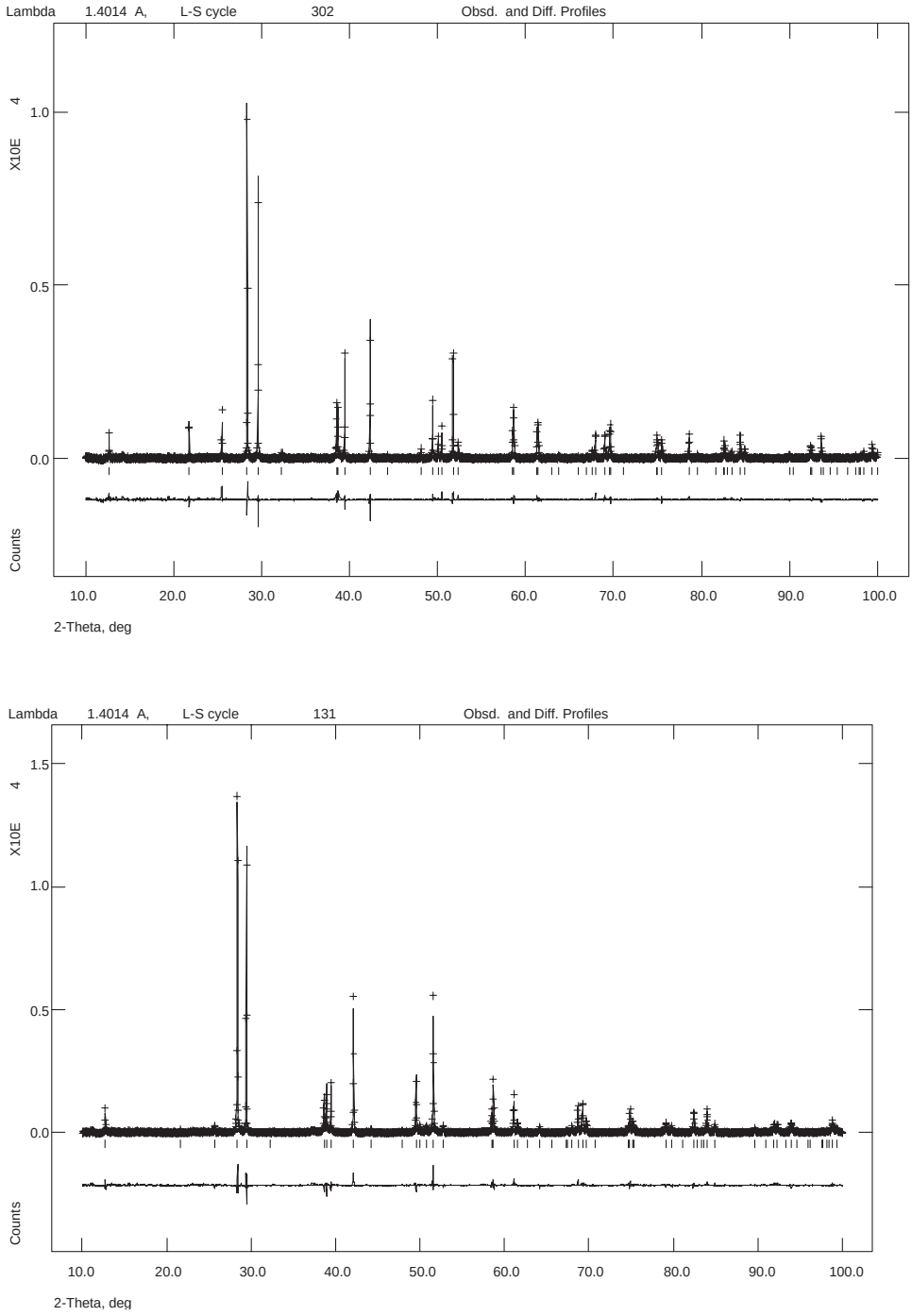

Fig. 1. Refined X-ray data for (a) $La_{0.8}Sr_{1.2}Fe_{0.9}Ru_{0.1}O_{4\pm\delta}$ and (b) $La_{0.2}Sr_{1.8}Fe_{0.6}Ru_{0.4}O_{4\pm\delta}$. R_{wp} = 9.82%, R_p = 7.46% and R_{wp} = 9.53% and R_p = 7.47%, respectively. + represents experimental data, solid line is the fit with the difference plot displayed beneath the plot.

Table 2
Cell constants refined from SRS data

Ru content (%)	a (Å)	c (Å)
10	3.88087(2)	12.69903(7)
20	3.88700(1)	12.67625(6)
30	3.89390(2)	12.64467(12)
40	3.89903(2)	12.61727(9)

showed that, assuming a ruthenium oxidation state of +5, the average iron oxidation state is +3 for both samples but that there are localized areas where the iron oxidation state is between +2 and +3 and other areas where the iron oxidation state lies between +4 and +3. The Mössbauer data have been fitted using three doublet components for the spectrum, (Fig. 5 and Table 5) as fitting with one or two doublets was found

to be insufficient to adequately fit the data, resulting in implausible peak widths. For the two samples, 10% and 30% Ru doped, the major contributing doublets were centered at an isomer shift of 0.32 and 0.38 mm/s, respectively. This is consistent with an iron oxidation state of +3. The two remaining components, for example in the case of the 30% Ru doped material, lie at 0.55 and 0.21 mm/s. The higher isomer shift suggests an iron oxidation state of between +2 and +3 as Fe^{2+} is usually observed at around 0.96 mm/s at room temperature [19,20]. The lower isomer shift shows some Fe^{4+} character as the typical isomer shift of Fe^{4+} in other materials with an octahedral coordination environment has been reported at –0.16 mm/s at ambient temperature [19,20]. All three components in each composition show similar quadrupole shifts (Table 5) indicating that the coordination environments are similar. These data therefore suggest that the electron density is not equally distributed throughout the structure and it may reflect the presence of ruthenium on the iron site.

The analysis of the Mössbauer spectroscopy data also highlights other structural points. There is a large change in the quadrupole shift (QS) as the stoichiometry is changed in the material. While the 10% Ru doped phase shows QS values for the three component doublets of around 1.0 mm/s, the 30% Ru doped phase has QS values of around 0.7 mm/s. This change reflects distortions in the (Fe/Ru)–O_6 octahedra within the material and is further supported by the earlier structural characterization. The more regular bond lengths observed in the structural studies correspond

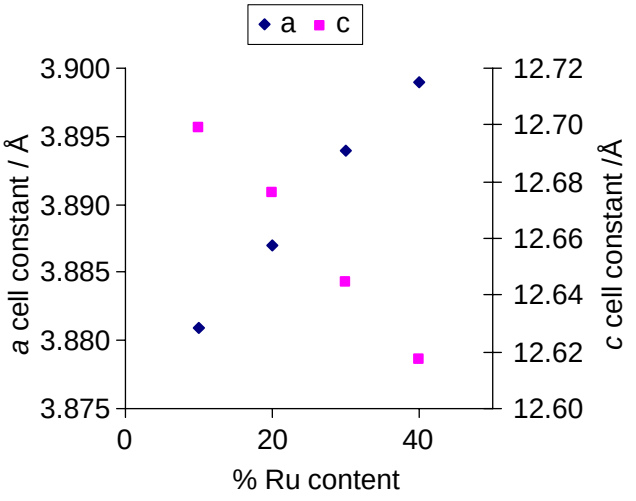

Fig. 2. Cell constants as a function of Ru content refined from synchrotron X-ray diffraction data (errors are within the data marker).

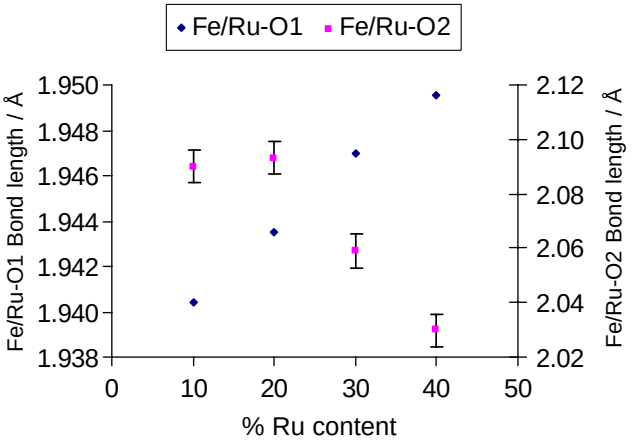

Fig. 3. Bond length variations for the (Fe/Ru)–O6 octahedra as a function of composition from synchrotron X-ray diffraction data.

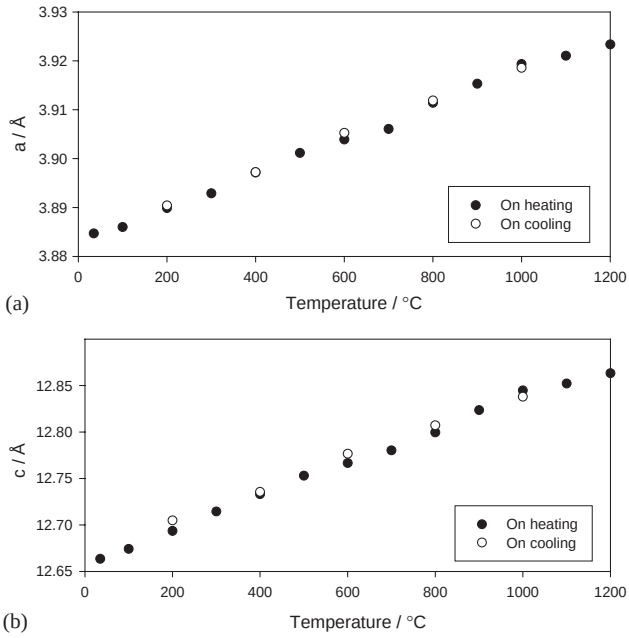

Fig. 4. (a) *a* cell constant and (b) *c* cell constant as a function of temperature as a for 20% Ru doped material.

Table 3
Bond lengths from SRS data

Ru content (%)	(Fe/Ru)–O1/Å	(Fe/Ru)–O2/Å	(La/Sr)–O1/Å	(La/Sr)–O2/Å	(La/Sr)–O2/Å
10	1.94044(1)	2.090(6)	2.6497(6)	2.7590(7)	2.455(6)
20	1.94350(1)	2.093(5)	2.6599(5)	2.7624(5)	2.429(6)
30	1.94695(1)	2.059(8)	2.6780(7)	2.7622(7)	2.429(8)
40	1.94952(1)	2.030(5)	2.6802(5)	2.7637(4)	2.439(5)

Table 4
Oxidation state analysis

Sample (%)	Mössbauer spectroscopy	Iodometric titrations	TGA (in H_2/N_2 up to 700°C)
10	$La_{0.8}Sr_{1.2}Fe^{IV}_{0.10}Fe^{III}_{0.73}Fe^{II}_{0.07}Ru^{V}_{0.10}O_{4.01}$	$La_{0.8}Sr_{1.2}Fe^{IV}_{0.07}Fe^{III}_{0.69}Fe^{II}_{0.15}Ru^{V}_{0.08}O_{3.93}$	0.11 O loss i.e. 0.1 Ru^{v} to Ru^{III}
20	N/A	$La_{0.6}Sr_{1.4}Fe^{IV}_{0.10}Fe^{III}_{0.62}Fe^{II}_{0.10}Ru^{V}_{0.19}O_{4.00}$	0.18 O loss i.e. 0.2 Ru^{v} to Ru^{III}
30	$La_{0.4}Sr_{1.6}Fe^{IV}_{0.10}Fe^{III}_{0.56}Fe^{II}_{0.04}Ru^{V}_{0.30}O_{4.10}$	$La_{0.4}Sr_{1.6}Fe^{IV}_{0.23}Fe^{III}_{0.46}Fe^{II}_{0.01}Ru^{V}_{0.30}O_{4.10}$	0.33 O loss i.e. 0.3 Ru^{v} to Ru^{III}
40	N/A	$La_{0.2}Sr_{1.8}Fe^{IV}_{0.24}Fe^{III}_{0.32}Fe^{II}_{0.04}Ru^{V}_{0.40}O_{4.10}$	0.39 O loss i.e. 0.4 Ru^{v} to Ru^{III} (all Fe^{III})

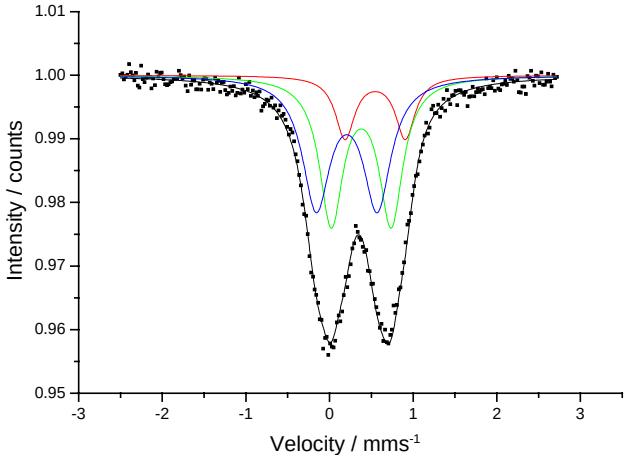

Fig. 5. Fitted ^{57}Fe Mössbauer spectrum of 30% Ru doped phase.

to the lower QS values observed in the Mössbauer spectra (Table 5 and Fig. 5).

Results obtained from iodometric titrations agree reasonably well with the Mössbauer spectroscopy results (Table 4). While the Ru maintains a +5 oxidation state and the average iron oxidation state is sustained at +3 there is evidence to suggest the presence of both Fe^{2+} and Fe^{4+} in these materials. This, as was observed with the Mössbauer spectroscopy data, suggests fluctuations in electron density throughout the sample. It may be evidence that the ruthenium is not distributed randomly in the material and that there are Ru-rich regions. Any iron in the vicinity of these regions will exhibit a lower oxidation state in order to maintain the charge balance. Further studies of these materials are underway to clarify this data analysis.

(ii) *Reduced samples*: In an attempt to investigate the oxygen stoichiometry of the ruthenium doped samples thermogravimetric analysis (TGA) data were collected on samples of each composition under reducing conditions. A gas of composition 10% H_2/N_2 was passed over the samples as they were heated to 1000°C at 10°/min. All of the samples showed a gradual mass loss that started at around 400°C. For each sample there was an initial rapid mass drop and subsequently the mass continued to slowly drop. A larger mass loss was observed for the samples with a higher ruthenium content and corresponds to a larger oxygen loss in these samples. X-ray diffraction was performed on the samples after the TGA analysis and it was found that while the K_2NiF_4 structure appeared to remain intact for the samples doped with 10% and 20% ruthenium on the iron site, for the 30% and 40% samples extra reflections appeared in the X-ray diffraction pattern and the relative intensities of the peaks changed significantly. However, on closer examination it was apparent that the samples had not broken down into their constituent oxides as might be expected under reducing conditions. The 20% and 40% Ru doped samples were therefore further investigated using high-temperature powder X-ray diffraction with a flow of H_2/N_2 over the sample in the diffraction chamber.

Data were collected at temperature intervals between room temperature and 1000°C. These experiments showed that while the K_2NiF_4 structure remains intact for the 20% Ru doped phase, a phase transition occurs as the temperature is increased for the 40% doped sample (Fig. 6(a)). On cooling the 40% Ru doped sample in H_2/N_2 this new phase was shown to be stable at room temperature. A further experiment heating the reduced sample in an air flow was then attempted. This experiment clearly illustrated that the phase transition was completely reversible as the tetragonal K_2NiF_4 structure recrystallized (Fig. 6(b)).

The powder X-ray diffraction data collected were subsequently analyzed using Rietveld refinement with the GSAS suite of programs [15]. The reduced phase with 20% Ru doping was refined in the space group *I4/mmm*, with the K_2NiF_4 structure, as previously described for the fully oxidized phases. The reduced phase for the 40% Ru doped sample has been successfully indexed as an orthorhombic distortion of the tetragonal structure. The peaks can be indexed in the space group *Immm* which is closely related to the tetragonal *I4/mmm* structure. Table 6 compares the initial atomic positions and refinement parameters used for the two structures. The refined cell constants obtained from the in situ X-ray diffraction data are given in Fig. 7 for the 20% doped material and Fig. 8 for the 40% doped material.

For the 20% Ru doped phase (Fig. 7) the *a* cell constant increased with temperature until a temperature of 300–400°C was reached where there was a sharp decrease in the magnitude to the cell constant. Above 400°C the cell constant increased once more but with a

Table 5
Summary of the fits tp Mössbauer data for 10% and 30% doped Ru materials

Sample	Component 1				Component 2				Component 3			
(%)	IS (mm/s^1)	QS (mm/s^1)	*W*	%	IS (mm/s^1)	QS (mm/s^1)	*W*	%	IS (mm/s^{-1})	QS (mm/s^{-1})	*W*	%
10	0.48 (1)	1.05 (1)	0.33 (1)	31.7 (2)	0.32 (1)	1.01 (1)	0.31 (1)	37.1 (2)	0.16 (1)	1.02 (1)	0.41 (1)	31.2 (2)
30	0.55 (1)	0.72 (1)	0.31 (1)	19.4 (2)	0.38 (1)	0.72 (1)	0.32 (1)	43.5 (2)	0.21 (1)	0.73 (1)	0.38 (1)	37.1 (2)

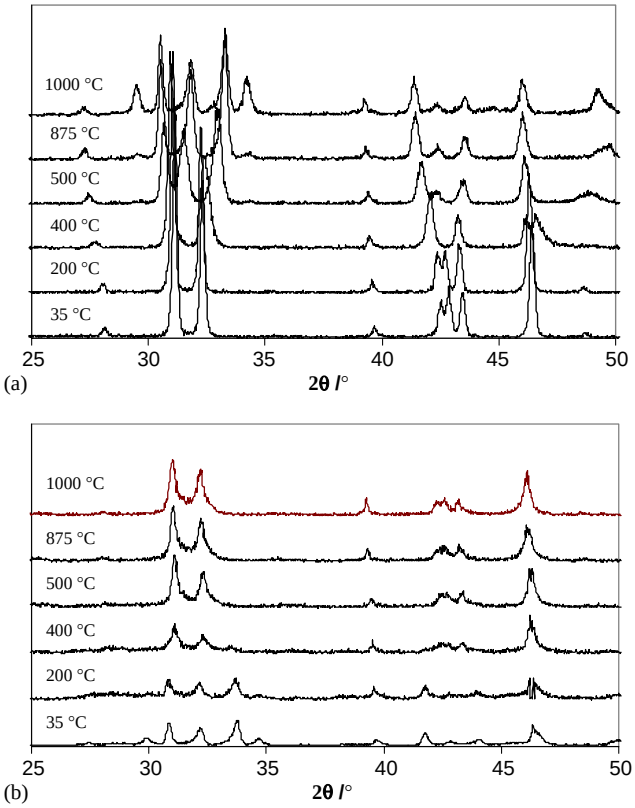

Fig. 6. (a) In situ X-ray diffraction patterns recorded during reduction of the 40% Ru doped phase, (b) In situ X-ray diffraction patterns recorded during reoxidation of the 40% Ru doped phase.

reduced thermal expansion coefficient. On re-oxidation the *a* cell constant markedly increased at between 300°C and 400°C. This temperature corresponds to that at which the major mass loss was observed in the TGA data under reducing conditions. The *c* cell constant showed similar effects with a discontinuity occurring at between 300°C and 400 °C on heating in the H_2/N_2 gas flow and then on re-oxidation in the same temperature range. Comparing the structures of the reduced and oxidized phases at room temperature, *a* is smaller for the reduced sample, while *c* is larger. These results are similar to those observed by Li and Greaves for the manganate, $La_{1.2}Sr_{0.8}MnO_{4\pm\delta}$ [21] where a range of stoichiometries were observed ranging between $La_{1.2}Sr_{0.8}MnO_{3.94}$ and $La_{1.2}Sr_{0.8}MnO_{4.27}$ Oxidation of the oxygen deficient manganate phase resulted in a 2.8% expansion of the *a* cell constant from 3.8270 to 3.9348 Å, while the *c* cell constant contracted by 4.2% from 13.0686 Å to 12.5238 Å, with the K_2NiF_4 structure being maintained throughout [21]. For the ruthenium doped phases discussed here the percentage changes are less dramatic. From synchrotron X-ray diffraction data collected, the refinements show that for the 10% Ru doped phase, *a* increased from 3.87367(1) to 3.88087(1) Å on oxidation, an expansion of 0.18%. The *c* cell constant was found to decrease from 12.73610(6) to 12.69902(7) Å, a contraction of 0.29%. The changes in the unit cell parameters observed here are clearly the result of the loss of oxygen from the structure and the reduced oxidation state of one or both transition metal ions.

In the case of the 40% Ru doped sample it was evident from the in situ X-ray diffraction data that the oxygen losses that occurred on heating were much larger than for the 20% Ru doped material. In this case the oxygen loss clearly was sufficient to drive a phase transition to occur but was not sufficient to result in a complete breakdown of the structure. Fig. 8 shows the variations in *a* and *c*, respectively, with temperature during heating in air and then in 10% H_2/N_2. Fig. 9 shows the effect of reduction on the cell volume.

To confirm the analysis of the in situ XRD investigations and the tentative assignment of the orthorhombic *Immm* space group further high-resolution X-ray data were recorded using the synchrotron X-ray source for these reduced samples. These data were fitted using the tetragonal *I*4/*mmm* model for 10% Ru doped sample and the *Immm* model for 30% and 40% Ru doped samples. No data was available for the 20% reduced sample. The 10% Ru doped sample refined with a tetragonal model gives an excellent fit to the data (Fig. 10) giving lattice parameters of $a = 3.87367(1)$ Å and $c = 12.73610(6)$ Å.

For the 30% Ru doped sample, peak broadening and subtle changes in relative peak intensities were evident on close inspection of the diffraction pattern and this phase is best described using the orthorhombic *Immm* model. There are three oxygen sites in the initial *Immm* model: O1 $(\frac{1}{2}0\frac{1}{2})$, O2$(0\frac{1}{2}\frac{1}{2})$ and O3 $(00z)$, $z \approx 0.16$. Oxygen loss in the 30% Ru doped material was found to occur almost exclusively from the O1 site. For this material the O1 site was only half occupied after reduction. This leads to an approximate stoichiometry of $La_{0.4}Sr_{1.6}Fe_{0.7}Ru_{0.3}O_{3.3}$. Details of the final refined

Table 6
Refined Rietveld parameters for reduced (a) 10% , R_{wp} = 9.34%, R_p = 7.14% and (b) 30% Ru doped material, R_{wp} = 11.56%, R_p = 8.70%

	x	y	z	$U_{iso} \times 100$ (Å^2)	O_{cc}	Mult.
(a)						
Sr	0	0	0.35792(6)	0.477(24)	0.415(12)	4
La	0	0	0.35792(6)	0.477(24)	0.585(12)	4
Fe	0	0	0	0.41(5)	0.923(8)	2
Ru	0	0	0	0.41(5)	0.077(8)	2
O1	0	0.5	0	0.78(17)	1	4
O2	0	0	0.1662(5)	1.35(16)	1	4
(b)						
Sr	0	0	0.35530(11)	0.90(5)	0.250(22)	4
La	0	0	0.35530(11)	0.90(5)	0.750(22)	4
Fe	0	0	0	0.57(8)	0.632(14)	2
Ru	0	0	0	0.57(8)	0.368(14)	2
O1	0	0	0.5	1	0.541(30)	2
O2	0.5	0.5	0.5	1	1	2
O3	0	0	0.1647(7)	0.63(23)	1	4

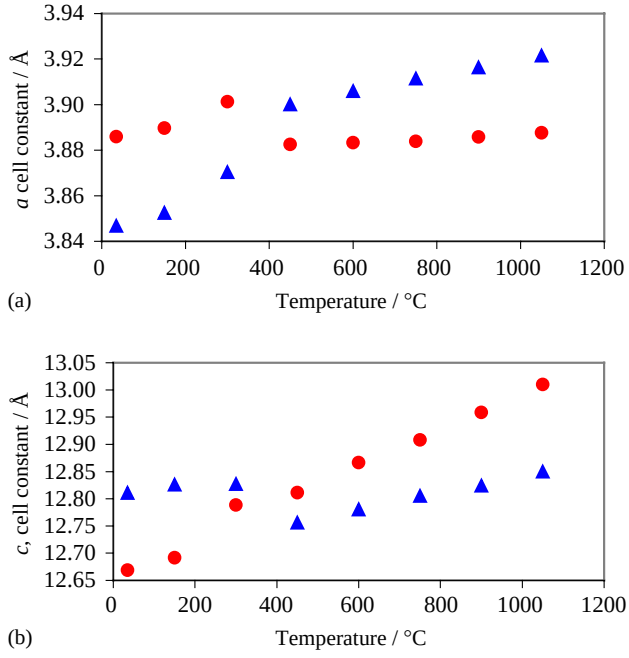

Fig. 7. (a) a cell constant and (b) c cell constant as a function of temperature during reduction (circles) and reoxidation (triangles) for the 20% Ru doped material.

atomic positions for 10% and 30% Ru doped materials are given in Table 6. The isotropic temperature factors of the O1 and O2 sites in the 30% doped sample were found to vary significantly and refined to unrealistic values. Hence a value of $U_{iso} \times 100 = 1.00$ was selected as a reasonable value and used as a fixed value in this data set. Refinement of the data for the 40% Ru doped sample proved difficult to achieve with the diffraction patterns broadened and also evidence of a secondary phase, possibly due to the onset of reoxidation, being

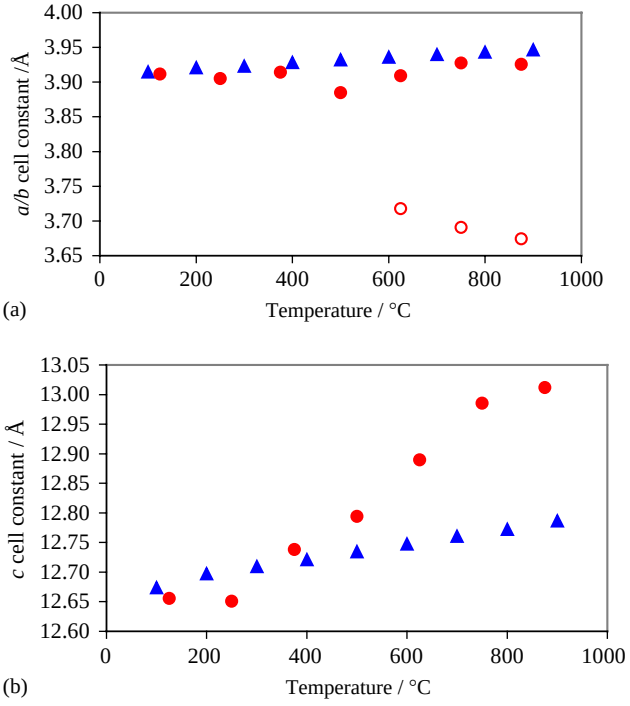

Fig. 8. (a) a cell constant and (b) c cell constant as a function of temperature during reduction (circles) and reoxidation (triangles) for the 40% Ru doped material.

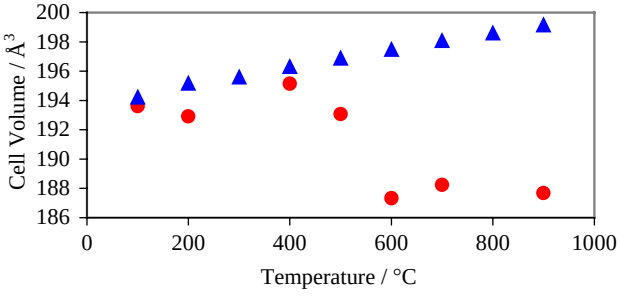

Fig. 9. Variation of cell volume during reduction (circles) and reoxidation (triangles) for the 40% Ru doped sample.

present. Therefore, although accurate determination of the lattice parameters ($a = 3.87983(13)$ Å, $b = 3.69637(15)$ Å and $c = 12.9121(5)$ Å) was possible further structural details are unavailable. To overcome these difficulties further work on the preparation of these highly reduced materials is ongoing and further structural studies using both high-resolution electron microscopy and neutron diffraction will be performed. In situ reduction of the 40% Ru doped phase during the diffraction experiment would be ideally required to give unequivocal information on this structure.

The *Immm* structure that would be adopted by the fully reduced phase (i.e. occupancy of O1 = 0) is depicted in Fig. 11 with the K_2NiF_4 structure for comparison. Comparing the structures of the reduced and oxidized phases there are a number of differences that are

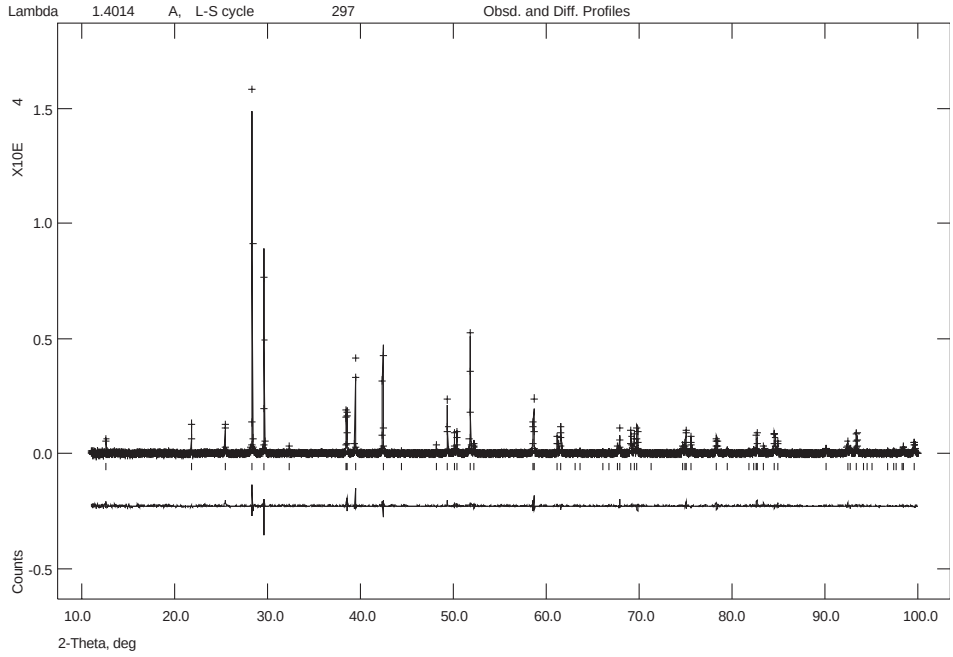

Fig. 10. Refined synchrotron X-ray diffraction data for reduced 10% Ru doped sample. R_{wp} = 9.34%, R_p = 7.14%.

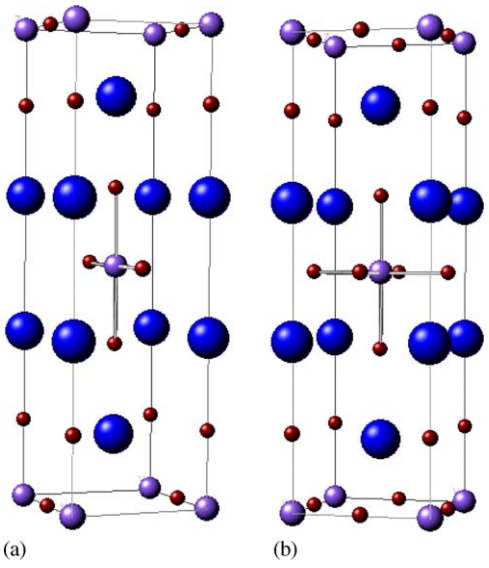

Fig. 11. Comparison of (a) *Immm* structure and (b) I4/*mmm* structures. Large spheres represent *A* cation, small spheres *O* and the intermediate spheres represent the *B* cation.

immediately apparent. The two structures are clearly related with the orthorhombic model missing oxygen atoms from one site in particular which results in a square planar type of coordination environment for the transition metal atoms. Other transition metal oxides that adopt this structure include Sr_2CuO_3 [22,23], Ca_2CuO_3 [22,23], Sr_2PdO_3 [24], Ba_2PdO_3 [25], Ba_2CuO_3 [26] and $Ba_2CuO_{3.39}$ [22,23]. To our knowledge the reported *Immm* structure is unique in iron or ruthenium chemistry. Of course, the possibility of some degree of ordering of the Fe and Ru cannot be discounted as contributing to the unusual coordination environment. Mössbauer spectroscopy of the reduced phases as well as further detailed structural studies would be desirable.

The reduced phase can be made in a furnace by heating the oxidized phase at 700°C under flowing H_2/N_2 (10% H_2) for 6 h then cooling to room temperature. The reduced phase is stable for several days in air but then begins to degrade. There seems to be some oxidation but also some decomposition that could be the result of moisture attacking the structure.

4. Conclusions

New phases of composition $La_{0.8}Sr_{1.2}Fe_{0.9}Ru_{0.1}O_{4\pm\delta}$, $La_{0.6}Sr_{1.4}Fe_{0.8}Ru_{0.2}O_{4\pm\delta}$, $La_{0.4}Sr_{1.6}Fe_{0.7}Ru_{0.3}O_{4\pm\delta}$ and $La_{0.2}Sr_{1.8}Fe_{0.6}Ru_{0.4}O_{4\pm\delta}$ have been synthesized using solid-state chemical techniques. These phases were found to adopt the tetragonal K_2NiF_4-type structure and were stable at least up to temperatures of 1000°C in air.

Investigation of the stability of these phases in reducing atmospheres indicated that there was a significant loss of oxygen from the structure. For 10% and 20% Ru doped phases this simply results in a tetragonal K_2NiF_4 phase with new cell parameters reflecting the stoichiometry and oxidation state changes. For the 30% and 40% Ru doped phases a larger loss of oxygen results in a phase transition to a new orthorhombic structure crystallising in the space group *Immm*, which is related to the K_2NiF_4 structure but with oxygen

vacancies on a particular crystallographic site ($\frac{1}{2}0\frac{1}{2}$). This results in a reduced coordination sphere for the transition metal atoms and possibly even the unusual square planar coordination.

Acknowledgments

We thank the EPSRC for funding this work under Grant GR/N23233 which provided funding for AJJ and the CCLRC for providing access to the SRS facility under Grant 37101. Thanks are also due to Dr. Chiu Tang of Daresbury Laboratory for his assistance with the running of station 2.3.

References

[1] V.V. Kharton, A.P. Viskup, A.V. Kovalevsky, E.N. Naumovich, F.M.B. Marques, Solid State Ionics 143 (2001) 337.
[2] V.V. Kharton, A.P. Viskup, E.N. Naumovich, F.M.B. Marques, J. Mater. Chem. 9 (1999) 2623.
[3] S.J. Skinner, J.A. Kilner, Solid State Ionics 135 (2000) 709.
[4] L. Minervini, R.W. Grimes, J.A. Kilner, K.E. Sickafus, J. Mater. Chem. 10 (2000) 2349.
[5] E. Boehm, J.-M. Bassat, F. Mauvy, P. Dordor, J.-C. Grenier, M. Pouchard, in: Forum, A.J. McEvoy (Ed.), Fourth ESOFC Proceedings of the fourth European Solid Oxide Fuel Cell Forum, Lucerne, 2000, p. 717.
[6] J.-M. Bassat, E. Boehm, J.-C. Grenier, F. Mauvy, P. Dordor, M. Pouchard, in: J. Huijsmans (Ed.), Fifth ESOFC Forum, Proceedings of the fifth European Solid Oxide Fuel Cell Forum, Lucerne, 2002, p. 586.
[7] A.J. Jennings, S.J. Skinner, J. Solid State Chem. (2002), submitted.
[8] P.D. Battle, S.K. Bollen, A.V. Powell, J. Solid State Chem. 99 (1992) 267.
[9] R. Greatrex, N.N. Greenwood, M. Lal, Mater. Res. Bull. 15 (1980) 113.
[10] S. Ebbinghaus, A. Reller, Solid State Ionics 101–103 (1997) 1369.
[11] K.W. Hyung, T.Y. Kwon, Y. Jeon, Solid State Commun. 125 (2003) 259.
[12] P.D. Battle, T.C. Gibb, C.W. Jones, F. Studer, J. Solid State Chem. 78 (1989) 281.
[13] S. Fujihara, T. Nakata, H. Kozuka, T. Yoko, J. Solid State Chem. 115 (1995) 456.
[14] M. Shimada, M. Koizumi, Mat. Res. Bull. 11 (1976) 1237.
[15] A.C. Larson, R.B. Von Dreele, General structure analysis system, Los Alamos National Laboratory, 1995.
[16] J.L. Soubeyroux, P. Courbin, L. Fournes, D. Fruchart, G. Le Flem, J. Solid State Chem. 31 (1980) 313.
[17] J.B. Goodenough, G. Demazeau, M. Pouchard, P. Hagenmuller, J. Solid State Chem. 8 (1973) 313.
[18] A. Le Bail, H. Duroy, J.L. Fourquet, Mat. Res. Bull. 23 (1988) 447.
[19] N.N. Greenwood, T.C. Gibb, Mössbauer Spectroscopy, Chapman & Hall, London, 1971.
[20] T.C. Gibb, J. Mater. Chem. 2 (1992) 415.
[21] R.K. Li, C. Greaves, J. Solid State Chem. 153 (2000) 34.
[22] D.R. Lines, M.T. Weller, D.B. Currie, D.M. Ogborne, Mater. Res. Bull. 26 (1991) 323.
[23] M.T. Weller, D.R. Lines, J. Solid State Chem. 82 (1989) 21.
[24] H.D. Wesel-Nielen, R. Hoppe, Z. Anorg. A C A 375 (1970) 209.
[25] Y. Laligant, A. Le Bail, G. Ferey, M. Hervieu, B. Raveau, A. Wilkinson, A.K. Cheetham, Eur. J. Solid State Chem. 25 (1988) 237.
[26] W.K. Wong-Ng, K.L. Davis, R.S. Roth, J. Am. Ceram. Soc. 71 (1988) C64.